



HAL
open science

Extreme hydrological regimes of a small urban river: impact on trace element partitioning, enrichment and fluxes

Gaël Durrieu, Nicolas Layglon, Sébastien D'onofrio, Benjamin Oursel, Dario Omanović, Cédric Garnier, Stéphane Mounier

► **To cite this version:**

Gaël Durrieu, Nicolas Layglon, Sébastien D'onofrio, Benjamin Oursel, Dario Omanović, et al.. Extreme hydrological regimes of a small urban river: impact on trace element partitioning, enrichment and fluxes. *Environmental Monitoring and Assessment*, 2023, 195 (9), pp.1092. 10.1007/s10661-023-11622-x . hal-04477486

HAL Id: hal-04477486

<https://hal.science/hal-04477486v1>

Submitted on 26 Feb 2024

HAL is a multi-disciplinary open access archive for the deposit and dissemination of scientific research documents, whether they are published or not. The documents may come from teaching and research institutions in France or abroad, or from public or private research centers.

L'archive ouverte pluridisciplinaire **HAL**, est destinée au dépôt et à la diffusion de documents scientifiques de niveau recherche, publiés ou non, émanant des établissements d'enseignement et de recherche français ou étrangers, des laboratoires publics ou privés.

1 Extreme hydrological regimes of a small urban river: impact on trace element partitioning, 2 enrichment and fluxes

3

4 Durrieu Gaël^{1,*}, Layglon Nicolas^{1,2}, D'Onofrio Sébastien¹, Oursel Benjamin³, Omanović Dario⁴, Garnier Cédric¹,
5 Mounier Stéphane¹

6

7 ¹Université de Toulon, Aix Marseille Univ., CNRS, IRD, MIO, Toulon, France

8 ²University of Geneva, Sciences II, 30 Quai E.-Ansermet, 1221 Geneva 4, Switzerland

9 ³Aix Marseille Univ., Université de Toulon, CNRS, IRD, MIO, Marseille, France

10 ⁴Center for Marine and Environmental Research, Ruđer Bošković Institute, P.O. Box 180, 10002 Zagreb, Croatia

11 *Corresponding author: gael.durrieu@univ-tln.fr

12 ORCID : Durrieu Gaël : 0000-0002-1917-7530; Layglon Nicolas : 0000-0001-7731-1067 ; Oursel Benjamin : 0000-
13 0002-1065-9146 ; Omanović Dario : 0000-0001-5961-0485 ; Garnier Cédric : 0000-0002-5638-6673 ; Mounier
14 Stéphane : 0000-0002-9624-0230

15 Email addresses : Durrieu Gaël : gael.durrieu@univ-tln.fr ; Layglon Nicolas : Nicolas.Layglon@unige.ch ; D'Onofrio
16 Sébastien : sebastien.donofrio83@gmail.com ; Oursel Benjamin : benjamin.oursel@mio.osupytheas.fr ; Omanović
17 Dario : omanovic@irb.hr ; Garnier Cédric : cgarnier@univ-tln.fr ; Mounier Stéphane : stephane.mounier@univ-tln.fr

18 Abstract

19 The input of trace elements from a small urban river (Las River, Toulon, France) located on the northern Mediterranean
20 coast was studied during both base flow and flood events. A two-year monitoring period of water flow and suspended
21 particulate matter (SPM) showed a typical Mediterranean hydrological regime: a strong increase in water flow and SPM
22 during short flood periods. During the flood event, an up to 2-fold increase in dissolved trace element (D_{TM})
23 concentrations and particulate trace element content in SPM (P_{TM}) was observed compared to the baseline discharge.
24 The enrichment factor of elements in the SPM ranges from low or moderate for Co, Ni and Cr (1.0 – 4.7) to extremely
25 high for Cd (157). However, the enrichment factors decrease from base flow to flood, indicating a dilution effect with a
26 large yield of weathering particles with higher particle size. The most significant total trace element loading occurred
27 during flood, ranging from 78 % for As and Ni to 91 % for Pb, while P_{TM} loading during flood ranged from 35 % for As
28 to 77 % for Pb. The specific dissolved fluxes during the flood are significantly higher for Pb, Cu and Zn than in the
29 surrounding rivers, indicating specificity in the catchment (lithology). This study shows the importance of monitoring
30 the transport of pollutants through small urban rivers and their potential impact on the coastal region, especially when
31 they enter small and closed bays, as a receiving pool.

32

33 **Keywords:** small river; trace metals; urban impact; Extreme event

34

35 Statements and Declarations

36 Funding

37 This study was part of the METFLUX research project funded by the French water agency “Agence de l’Eau Rhône
38 Méditerranée Corse” (convention n°2016-1364).

39 Competing Interests

40 The authors have no relevant financial or non-financial interests to disclose.

41 Data availability

42 The datasets generated and analysed during the current study are available from the corresponding author on reasonable
43 request.

44 Author Contributions Statement

45 Garnier Cédric conceptualized the study and acquired the funding. Mounier Stéphane and Garnier Cédric oversaw the
46 project administration. Durrieu Gaël, Layglon Nicolas, D’Onofrio Sébastien, Oursel Benjamin, Omanović Dario,
47 Garnier Cédric and Mounier Stéphane participated in the sampling, the analyses and the revision of the original
48 manuscript. Durrieu Gaël, Omanović Dario and Mounier Stéphane wrote the original manuscript.

49 Acknowledgments

50 The authors wish to thank “Météo-france” for the access to data from station “la Mitre”, Amonda El Houssainy for
51 helping create the map used and the LASEM (Laboratoire d’Analyses de Surveillance et d’Expertise de la Marine) in
52 Toulon for major elements analysis. The authors also thank the PACEM-MIO platform for facilities.

53 This work is dedicated to our friend and colleague Cédric Garnier (1977–2018). We will always remember him with
54 gratefulness.

55

56 Introduction

57 Rivers are known to be an important transport route for pollutants from the continent to coastal areas (Viers et al.,
58 2009). Overall, river runoff is the main source of metals and metalloids entering the waters of the continental shelf
59 (Olías et al., 2006; Viers et al., 2009) and therefore the transport of most contaminants depends on the runoff, resulting
60 from the precipitation regime in the river basin. The meteorological regime of the Mediterranean area is characterised
61 by long dry summers and mild winters. Long periods without rain (with accumulation of contaminants on the surfaces
62 of the catchment areas) are very often interrupted by short but intense rainfalls (Bernal et al. 2013; Cowling et al., 2005;
63 Miller, 1983) during which urban runoff, erosion and sediment resuspension occur. Consequently, water quality is
64 known to be affected by elevated trace metal concentrations (Cobelo-García et al., 2004; Nicolau et al., 2012; Oursel et
65 al., 2014). Another characteristic of flash flooding in Mediterranean regions is that it brings with it a considerable
66 amount of suspended matter of natural or anthropogenic origin, which serves as a vector for trace metals ,(Dumas et al.,
67 2015; Meybeck, 2001; Pont et al., 2002). This particular system requires an adapted sampling protocol to take into
68 account the actual pollutant load. The large fluctuations in precipitation lead to extreme variations in runoff and thus in
69 the fluxes of chemical elements. As a result, high-frequency sampling is required during flood events (intraday
70 frequency), while regular sampling (weekly or monthly) is sufficient during baseflow. Furthermore, understanding the
71 relationships between catchment characteristics (bedrock and lithology), anthropogenic activities (land use in the
72 catchment) and river flow (dam discharges and precipitation) is crucial for developing spatial models for trace metals in
73 a temperate continental shelf such as the Toulon Bay (France) (González-Ortegón et al., 2019). Moreover, small rivers
74 play an important role in the coastal zone of the Mediterranean because of their number (Nicolau et al., 2012; Roussiez
75 et al., 2011). Therefore, it is particularly important to ensure a good assessment of metal fluxes in urbanised coastal
76 areas, as they contribute significantly to the total amount of trace metals in the environment. Furthermore, when inputs
77 occur in a semi-enclosed bay, metal inputs can lead to a contamination gradient due to low tides and low water

78 turnover. In Toulon Bay (France), for example, there is a strong gradient of metal contamination in the sediments
79 (Tessier et al., 2011) for which it was found to affect benthic prokaryotic diversity (Misson et al., 2016) and has
80 implications for the quality of mussels farmed in the bay (Dang et al., 2015). Sediment resuspension has been shown to
81 influence the chemical and biological quality of Toulon Bay (Layglon et al., 2020). In the same bay, a high gradient of
82 dissolved trace metals in the water column was found to impact bacterioplanktonic and phytoplanktonic communities
83 (Coclet et al., 2018, 2019, 2020; Layglon et al., 2020). This gradient could be also due to the river input like the Las
84 river which is first rural and then becomes more urbanized along its crossing (Dufresne 2014). Since the watershed is
85 not much industrialized and the municipalities crossed fairly well cleaned up the quality of the river water should be
86 good even though not much information are available concerning this river. That's why, until now, it is unclear what is
87 the most important driver in bay contamination: river inputs, sediment resuspension, aerosol or river inputs.

88 The annual fluxes of contaminants to the coastal region by rivers are commonly estimated based on average level of
89 contaminants concentration and average river discharge. However, the dynamics of the fluxes, i.e. base flow vs. flood
90 events, was not always considered due to the logistical problems. Hence, the Las River (Toulon, France) was used as a
91 model of a small Mediterranean urban river characterised by extreme hydrological regimes due to the episodic heavy
92 rain events. This work aimed to (i) Characterise the inputs of trace metals during base flow and flood events, to
93 (ii) estimate the contribution of these inputs to the bay.

94 **Materials and methods**

95 **Site description**

96 The Las River is an 8 km long urban river located in south-eastern France near the city of Toulon on the north-western
97 coast of the Mediterranean Sea. Its catchment is located in a predominantly calcareous area (Baudement et al., 2017). In
98 the upper part it is mainly composed of forest, small agricultural zones and two stone quarries and in the lower part it is
99 urbanised. The area of the catchment is estimated at 60 km², but due to the karst type, water from another aquifer can
100 enter in the watershed (Dufresne, 2014; Lamarque, 2014). It starts at an altitude of 100 m after the Dardennes dam
101 (43°10'29.23" N; 5°55'49.13" E) which is used for drinking water supply, but also causes karst flash floods
102 downstream in the urban area (Baudement et al., 2017). The bed of the river consists in coarse gravel and crushed stone
103 (Dufresne et al. 2020). In the middle course, the Las River is channelised with concrete and covered over a length of
104 about 2 km. The river flows into the sea in the little bay of Toulon (43°6'58.11" N; 5°53'27.81" E) within a military
105 zone. This little bay is a semi-enclosed bay of about 9.1 km² characterized by an average depth of 10 m and separated
106 from the large bay by a dyke.

107 The rainfall regime of the region is Mediterranean and is subject to high (inter)annual variability. For example,
108 precipitation in Toulon averaged 670 mm in 2013-2018, with a minimum of 270 mm in 2017 and a maximum of 1120
109 mm in 2014 (Météo France, La Mitre station), and most rain occurred from October to April.

110

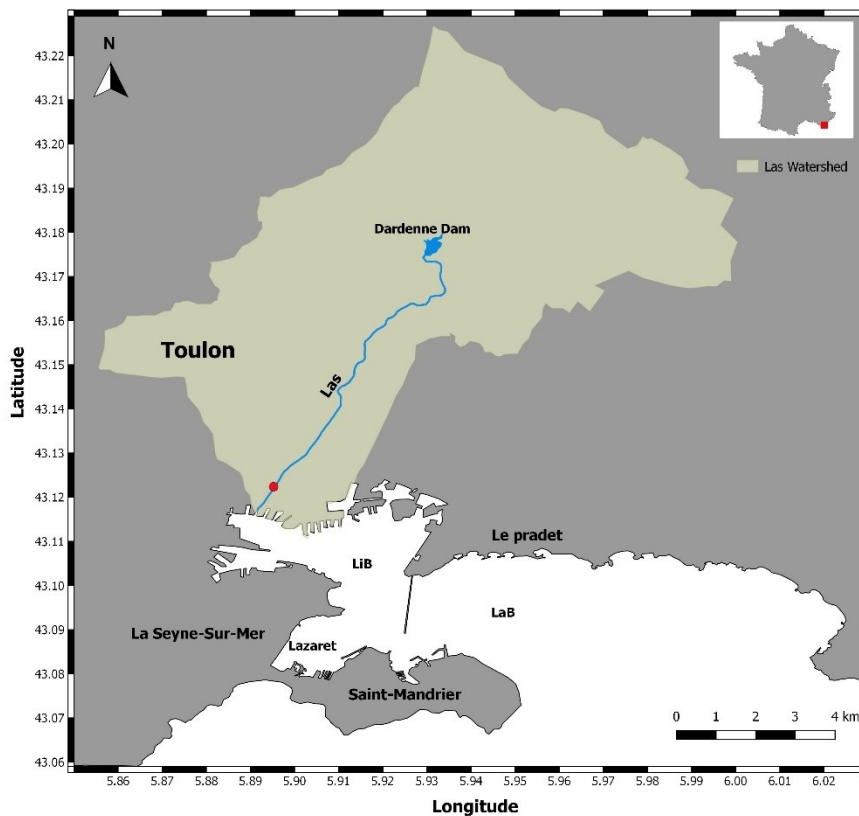
111 **Sampling**

112 To consider the most important part of the river, the sampling point (43°7'22.44" N; 5°53'44.20" E) is located 900 m
113 before the confluence with the sea (Fig. 1). To our knowledge, there are no further water inflows after this point.

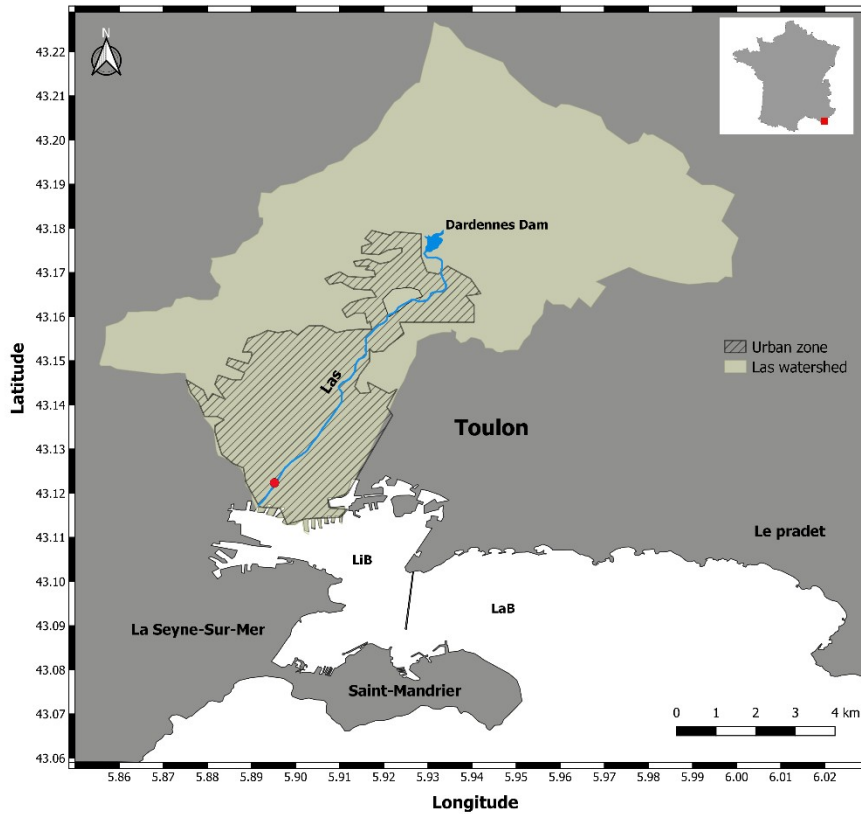
114 The sampling strategy consisted in sampling during base flow and flood events, using the passive and manual sampling
115 of suspended particulate matter and water. Sensus Ultra (ReefNet Inc.) loggers were used to monitor the water column

116 pressure (depth) and temperature (at 10 min intervals) in the period from March 2017 to March 2019, while a multi
117 parameters probe (600-OMS-V2, YSI) was additionally used to monitor turbidity, conductivity, depth and temperature
118 in the period from January 2018 to March 2019.

119 Before sampling, all FEP (Fluoro Ethylene Propylene) and HDPE (High Density Polyethylene) sampling bottles
120 (Nalgene) were cleaned with 10 % v/v HNO₃ (Fisher scientific, Analytical Reagent grade), rinsed 3 times with Milli-Q
121 water (resistivity 18.2 MΩ; Milli-Q Direct 8, Millipore) and filled with Milli-Q water acidified with 0.1 % HCl (Carl
122 Roth, Rotipuran supra) until sampling. Glass bottles (Wheaton 24 mL) and a glass filtration system were cleaned with
123 10 % v/v HCl (Fisher scientific 37 %, Analytical Reagent grade), rinsed 3 times with Milli-Q water before being
124 combusted for 6 h at 450 °C. Glass fibre filters (Whatman GFF, 0.7 μm) were combusted for 6 h at 450 °C, placed in an
125 oven (60 °C) until constant weight was measured.



126



127

128 **Figure 1.** The Las River catchment area (green) and sampling station (red point). LiB= little Bay, LaB = Large Bay

129

130 The strategy of sampling needed to combine a long-term monitoring of the river during the base flow and punctual
 131 sampling of flood events. For that purpose, during base flow samples were taken every month to cover the seasonal and
 132 temporal variability. The detail sampling of the major flood event monitored on 10/10/2018 is described below.

133

134 *Sampling during the base flow*

135 In total, 24 monthly sampling campaigns were conducted under base flow conditions from 20/2/2017 to 20/2/2019. For
 136 each campaign, 4 L of water was taken directly in the stream (after rinsing the sampling bottle 3 times with the stream
 137 water) for dissolved and particulate fraction analysis. In addition, using two deployed loggers and a YSI probe, the main
 138 physico-chemical parameters (temperature, specific conductivity, redox, pH, chlorophyll-a), were punctually measured
 139 each time using the Hydrolab DS5 multi-probe.

140 *Sampling during the flood event*

141 The strong rainy event (94 mm rain in 24 h, Météo France, La Mitre) occurred on 10/10/2018 was selected as a
 142 representative flood event. Samples were collected in a period from 11 h UTC to 24 h UTC. A precleaned HDPE bucket
 143 with a rope was used to collect river water from the bridge (43°7'22.44" N; 5°53'44.20" E). An integrative sampling
 144 strategy was used: depending on river discharge, estimated by water height, every 10 min during 1 h or every 20 min
 145 during 2 h, an aliquot of (1) 150 mL of bulk water was pooled in a 1 L HDPE bottle for further analysis of particulate
 146 material and (2) a 60 mL of sample was filtered using a 0.2 µm cellulose acetate (CA) syringe filter (Minisart,

147 Sartorius) and pooled in a 0.5 L FEP bottle for analysis of dissolved trace elements. In this way, a total of 11 composite
148 samples of (1) bulk (unfiltered) water and (2) filtered water were collected during the whole flood event.

149

150 Time-Integrated Suspended Particulate Matter (SPM_{TI}) sampling

151 A sediment trap (Phillips et al. 2000) made of a stainless-steel tube of 1 m length and 98 mm internal diameter (Fig. SI
152 1, in Supplementary Information) was used to continuously collect suspended particulate matter (SPM_{TI}). The details
153 about the sample and principle of the work are provided by Phillips et al. (2000). In short, water entered into the
154 sampler through a 4 mm hole facing towards the water stream. Due to the increase of the internal diameter of the tube,
155 an internal flow of the water was suddenly slowed down, allowing settlement of the particles inside of the tube. The
156 sediment trap is designed to collect SPM_{TI} at small streams. The period of deployment was adjusted depending on
157 meteorological conditions (from some days during flood to 1.5 month during base flow) to finally get a set of SPM_{TI}
158 corresponding to contrasted flow periods (12 samples under base flow and 5 samples under flood). The whole quantity
159 of water and SPM_{TI} in the trap was transferred in a 10 L HDPE bottle. After one day of sedimentation in a cold place,
160 supernatant was removed and SPM_{TI} was placed in a 150 mL HDPE bottle, frozen and freeze-dried thereafter.

161 Calculation of river flow

162 The determination of the flow is a key parameter when studying river inputs. In order to precisely determine the water
163 height of the river, two devices were used: a limnometer and a pressure sensor. The first device gives the official water
164 height certified by authorities (H_{Limn}) and the second one gives a high frequency measurement of water pressure (P_{sensor}).
165 Water pressure from the sensor was measured every 10 min and was corrected by the daily average atmospheric
166 pressure from Météo France services and transformed into water height (H_{sensor}). By using the certified measurement, a
167 linear regression ($R^2=0.98$, $N=12$) was done between H_{Limn} and H_{sensor} and used to transform all the H_{sensor} into H_{Limn} .
168 From this extended H_{Limn} data set, the rating curve established by (Lamarque 2014) was used to obtain the high
169 frequency river discharge. This rating curve has been validated for limnometer heights between 0.35 m to 1.85 m which
170 corresponds to the heights measured during our monitoring. In accordance with previous study from (Dufresne et al.
171 2020), the threshold of $1 \text{ m}^3 \text{ s}^{-1}$ was defined as the limit between base flow and flood. Table SI 2 summarizes the flows
172 during the different sampling campaigns.

173

174 High frequency suspended particulate matter (SPM_{HF}) determination

175 Another key parameter when studying river inputs is the SPM concentration. As shown previously, this parameter is
176 highly correlated to the turbidity (Dufresne, 2014; Dufresne et al., 2020). This property is used to estimate SPM from
177 high frequency measurement of turbidity probe, calibrated by using discrete SPM measurement from GFF filtration
178 (SPM_{GF}). First, the data outliers due to sensor clogging were replaced using a specific filter described in Fig. SI 3.
179 Secondly, turbidity > 1 NTU was transformed in SPM_{HF} by using the linear relation between SPM_{GF} values and
180 corresponding turbidity measurement ($R^2=0.98$, $N=20$). This concerns 25 % of the data set. Thirdly, for low turbidity, <
181 1 NTU or “nd” or data associated to flow < $1 \text{ m}^3 \text{ s}^{-1}$, the average of all measured SPM_{GF} concentration during base flow
182 was applied ($\text{SPM}_{\text{HF}} = \text{avg}(\text{SPM}_{\text{GF}}) = 1.13 \pm 0.34 \text{ mg L}^{-1}$). This concerns 69 % of data set. Finally, for turbidity <
183 1 NTU or “nd” associated to a flow > $1 \text{ m}^3 \text{ s}^{-1}$, as it is not base flow measurement, a specific linear relation ($R^2=0.81$,
184 $N=16$) between SPM_{GF} and flow was used to avoid underestimation of SPM_{HF}. This concerns 6 % of data set. The final
185 data contains $N = 103,282$ SPM_{HF} data between 2017 and 2019.

187 Filtration, treatment and preservation of samples

188 Samples for dissolved organic carbon (DOC) analysis were filtered at the laboratory using a 25 mm glass fibre filter
189 (Whatman GFF, 0.7 μm) during the base flow, whereas during the flood an in-line 0.2 μm cellulose acetate syringe
190 filter (Minisart, Sartorius) was used for on-site samples filtration. Before taking the final sample, the syringe filter was
191 rinsed several times with the ambient water (washed in this way, the blanks of DOC in Milli-Q were negligible). The
192 filtrates were collected in 24 mL pre-combusted glass tubes (Wheaton), preserved with 0.2 % HCl (Carl Roth 37 %
193 Rotipuran supra) and stored at 4 °C before analysis. The GFF filters were used to measure particulate organic carbon
194 (POC) and SPM_{GF} concentrations. Filters were dried overnight in an oven at 60 °C and thereafter stored at room
195 temperature in a closed box with a drying agent before weighting for SPM_{GF} content. For POC analysis, the GFF filters
196 were exposed to HCl fumes during 4 h in a glass desiccator to remove inorganic carbon, and after that stored in a fume
197 hood during 3 h and overnight in an oven at 60 °C before analysis (Lorrain et al. 2003).

198 For analysis of dissolved trace metals (D_{TM}), samples were filtered at the laboratory by using cellulose acetate filters
199 (47 mm, 0.2 μm , Sartorius) during the base flow. Before filtration, the filters were cleaned with 100 mL of 10 % v/v
200 HNO_3 (Fisher scientific, Analytical Reagent grade), then with 1 L Milli-Q water acidified with 0.1 % HCl (Carl Roth
201 37 %, Rotipuran supra) and finally rinsed with Milli-Q water. Then, the filtrate was collected in an 8 mL HDPE bottle
202 and preserved with 0.5 % HNO_3 (Carl Roth 69 %, Rotipuran supra) for further ICP-MS measurement of D_{TM} . During
203 periods of flooding, samples for dissolved fractions were filtered on-site by using in-line 0.2 μm cellulose acetate
204 syringe filters (Minisart, Sartorius). In-line syringe filters were cleaned by filtering 2 x 60 mL of 0.1 % v/v HNO_3
205 (Fisher scientific, Analytical Reagent grade), and then 2 x 60 mL of river water. After filtration in the field, the filtrate
206 was split for D_{TM} and major analysis. For analysis of particulate trace metals (P_{TM}) and SPM concentrations, water was
207 filtered at the laboratory using cellulose acetate filters (47 mm, 0.2 μm , Sartorius).

208 All filters from base flow and flood samples filtration were placed overnight in an oven at 60 °C and then placed 1 h in
209 an oven at room temperature with a drying agent before weighing. Both GFF and cellulose acetate filters were used to
210 determine SPM concentration (mg L^{-1}) in discrete samples (further denoted as SPM_{GF}).

211 Cellulose acetate filters (47 mm, 0.2 μm , Sartorius) and SPM_{TI} (see section 2.3) were mineralised by microwave
212 digestion (Milestone, UltraWAVE ECR) for the determination of trace element concentrations in particulate and solid
213 samples. Filter or 100 mg of SPM_{TI} were placed in a 15 mL teflon tube with aqua regia (mixture of 7.5 mL HCl and
214 2.5 mL of HNO_3 (Carl Roth, Rotipuran supra) and mineralized (temperature range from ambient to 240 °C in 20 min
215 and hold during 20 min, while pressure ranges from 30 bar to around 70 bar). After digestion the whole volume of
216 digestate was transferred in a 30 mL HDPE bottle and diluted to a final volume of 25 mL for further ICP-MS
217 measurement of particulate trace metals (P_{TM}). The P_{TM} was then expressed in trace metal content in $\mu\text{g g}^{-1}$ of SPM
218 using SPM_{GF} or SPM_{TI} .

219

220 Analysis of parameters

221 *DOC*

222 DOC was determined by high temperature combustion at 720 °C using a TOC-V Analyser (Shimadzu®), calibrated
223 using potassium hydrogen phthalate standard. The limit of quantification is 0.1 mgC L^{-1} with a good linearity from 0.1

224 to 50 mgC L⁻¹. Quality control (QC) of measurements was checked every run by the determination of element
225 concentration in “a Lake Water Reference Material” (SUPER-05, Environment and Climate Change Canada). Certified
226 values for DOC is 1.28 mg_C L⁻¹. Obtained values for the whole data set agreed with certified values within 2 %.

227

228 *POC*

229 POC was determined using a Flash 2000 NC Soil Analyser (Thermo Scientific®). Carbon was measured by flash
230 combustion at 930 °C in tin capsules. The limit of detection was 5 µg, and the calibration curve ranges respectively
231 from 5 to 1100 µg. Quality control (QC) of measurements was checked by the determination of element concentration
232 in “NC Soil” (Thermo Fisher Scientific). Certified values for POC is 2.29 % C. Obtained values for the whole data set
233 agreed with certified values within 1 %. In the following text, POC concentration refers to mass of POC per volume of
234 water and POC content refers to mass of POC per mass of SPM.

235

236

237 *Trace elements*

238 D_{TM} and P_{TM} (Al, As, Cd, Co, Cr, Cu, Ni, Pb and Zn) were determined by High Resolution Inductively Coupled Plasma
239 Mass Spectrometer (HR ICP-MS, Element 2, Thermo Finnigan, Bremen, Germany). The samples for the analyses were
240 prepared in pre-cleaned polypropylene tubes (Sarstedt). Freshwater samples were analysed undiluted (acidified to 2 %
241 v/v HNO₃, ROTIPURAN Supra, Carl Roth), whereas an appropriate dilution (5-10×) for digested SPM_{GF} or SPM_{TI}
242 samples was used. Indium (¹¹⁵In) was used as an internal standard. Quality control (QC) was checked by the
243 determination of element concentration in “River Water Reference Material for Trace Metals” (SLRS-5, National
244 Research Council Canada) and PACS-2 for sediment samples.

245

246 *Calculation of parameters*

247 *Load of TM*

248 For the dissolved fraction, the calculation of the load (DL_{TM} in g) is defined as:

$$249 \quad DL_{TM} = \sum_{i=1}^n (V_i \times D_{TM,i} \times 10^{-3}) \quad \text{equation 1}$$

250 where DL_{TM} is the dissolved load of a given element (g) during observation 1 to *n*, D_{TM,i} is the dissolved concentration
251 of a given trace metal (µg L⁻¹) and V_i is the volume of river water (m³) between two observations *i* and *i*+1. We
252 distinguished two conditions for the load calculation. During the base flow (flow < of 1 m³ s⁻¹) D_{TM,i} concentration
253 corresponds to the concentration measured from the date of sampling (observation *i*) until the next sampling
254 (observation *i*+1). For unsampled flood events (flow > of 1 m³ s⁻¹), D_{TM,i} concentration was estimated from the
255 relationship between DL_{TM} and Q during the flood sampling on 10th October 2018. For the 8 studied elements the R²
256 coefficient varied between 0.86 and 0.98, depending on the element (SI 4).

257 The particulate fraction calculation of the load (PLTM) was defined as:

258

$$PL_{TM} = \sum_{i=1}^n \left(SPM_{Mass,i} \times P_{TM,i} \times 10^{-6} \right) \quad \text{equation 2}$$

259 where PL_{TM} is the particulate load of a given trace metal (g) during observation 1 to n , $P_{TM,i}$ is the content of a given
 260 trace metal during observation to $i+1$ ($\mu\text{g g}^{-1}$) in SPM_{TM} , $SPM_{Mass,i}$ is the mass of SPM_{HF} (g) during observation i to $i+1$.

261

262 *Enrichment factor (EF)*

263 To distinguish the lithogenic from an anthropogenic origin of trace metals in particles, enrichment factors were
 264 calculated. For that purpose, aluminium is assumed as a normalizer element and the concentration of the upper
 265 continental crust (UCC) proposed by Rudnick and Gao (2014) as the lithogenic background. The enrichment factor is
 266 calculated as follows:

267

$$EF_{TM,i} = \frac{\frac{P_{TM,i}}{P_{Al,i}}}{\frac{P_{TM,UCC}}{P_{Al,UCC}}} \quad \text{(equation 3)}$$

268 where $P_{TM,i}$ is the particulate content of a given element in SPM ($\mu\text{g g}^{-1}$) at observation i , $P_{Al,i}$ the aluminium content of
 269 the considered sample at observation i , $P_{TM,UCC}$ and $P_{Al,UCC}$ the element and aluminium content ($\mu\text{g g}^{-1}$) respectively in the
 270 UCC. To compare the degree of enrichment the classification defined by Sutherland (2000) was used. $EF < 2$:
 271 deficiency to low enrichment; $EF 2-5$: moderate enrichment; $EF 5-20$: significant enrichment; $EF 20-40$: very high
 272 enrichment; $EF > 40$: extremely high enrichment. In the present work for an element, EF_{TM} will represent the mean of
 273 EF_{flood} and $EF_{base\ flow}$ if no distinction is given.

274

275 *Distribution coefficient (K_D)*

276 To study the repartition of metals between the dissolved and the particulate fraction the distribution coefficient was
 277 calculated by the following equation:

278

$$K_{DTM,i} = \frac{P_{TM,i}}{D_{TM,i} \times 10^{-3}} \quad \text{(equation 4)}$$

279 where $K_{DTM,i}$ is the distribution coefficient (L kg^{-1}), $P_{TM,i}$ is the particulate content of a given element in SPM_{GF} ($\mu\text{g g}^{-1}$),
 280 as it is a punctual measurement, $D_{TM,i}$ is the dissolved concentration of the element ($\mu\text{g L}^{-1}$) at observation i . For each
 281 TM, an optimised $\log K_D$ during a flood or base flow is calculated using all $P_{TM,i}$ and $D_{TM,i}$ available from measured data
 282 using Excel Solver.

283

284 *Statistical analysis*

285 Microsoft Excel® XLSTAT add-on was used for statistical analyses. These tests were used to compare the data set for
 286 base flow versus for flood for each parameter. First, Grubbs' test was applied to remove extreme values (outliers). Then
 287 the Shapiro-Wilk test was applied to test the normality of each distribution. As all the distributions were not normally

288 distributed, the non-parametric test of Mann-Whitney (with a $p < 0.05$) was applied to determine differences between the
289 base flow and the flood data set.

290

291 **Results and discussion**

292 Main physico-chemical parameters

293 The average values of the main physico-chemical parameters (SPM, river flow, temperature, conductivity, dissolved
294 oxygen and chlorophyll-a) obtained for the base flow and flood events are presented in Table SI 5, along with data from
295 other similar water systems. A clear difference between the base flow and the flood was observed for SPM and the river
296 flow. The average increase by a factor 34 and 20 during the flood event was evidenced for SPM_{GF} and the flow,
297 respectively. Compared to other Mediterranean rivers (Table SI 5), the increase of SPM is slightly higher, regardless of
298 the watershed size, likely due to the Las River geology being composed of karstic rocks (Baudement et al., 2017).
299 Moreover, it should be highlighted that in these two years of study the flood occurred “only” 20 % of the time, but it
300 accounts for 69 % of the total water discharge and 78 % of the solid material yield. These results are close to ones
301 previously reported by (Dufresne, 2014; Dufresne et al., 2020) for the period October 2012 to January 2014 (flood 30 %
302 of the time, 85 % of the water discharge and 85 % of the solid material yield). Temperature, conductivity, dissolved
303 oxygen and pH remain stable regardless of the water regime. Chlorophyll-a is the only parameter that increases from
304 base flow to flood. This indicates an increase of phytoplankton abundance, however there is also a high probability that
305 the increase is related to the measurement artefact caused by high turbidity, which was often seen when the probe
306 touches the sediment.

307 Dissolved and particulate carbon concentrations

308 Average concentrations of organic carbon in dissolved and particulate phases are presented in Table 2. DOC
309 concentration is in the same range of other Mediterranean rivers from the same region, with a similar, 3-fold increase
310 during the flood over the base flow. POC concentrations are slightly smaller than other surrounding rivers mainly
311 because of a smaller SPM concentration (Table SI 5). The POC fraction ($POC / (DOC + POC)$) increased from 12 %
312 during the base flow to 47 % during the flood. Nevertheless, in terms of OC content in SPM, the values obtained in the
313 Las River are in the same range as the Huveaune, Jarret and Eygoutier Rivers, but higher than the Rhône River. For all
314 rivers OC content in SPM is 2-fold higher during the base flow compared to flood (Table 2). This trend is attributed to a
315 dilution of POC by addition of mineral particles resulting from erosion processes (Oursel et al., 2014).

316

317

318

319

320

321

322

323

324 **Table 2.** DOC (in $\text{mg}_C \text{L}^{-1}$), POC (in $\text{mg}_C \text{L}^{-1}$ and $\text{mg}_C \text{g}^{-1}$) in Las River during base flow and flood, Rhône River
 325 (Sempere et al., 2000), Huveaune and Jarret Rivers (Oursel et al., 2013; Oursel et al., 2014), Eygoutier River (Nicolau
 326 et al., 2012). For Las River, “§” refers to average and sd without extremes values, “*” refers to min-max values
 327 including extremes values.

328

		Dissolved	Organic Carbon Particulate	Particulate content
		$\text{mg}_C \cdot \text{L}^{-1}$	$\text{mg}_C \cdot \text{L}^{-1}$	$\text{mg}_C \cdot \text{g}^{-1}$
Las baseflow	□ average	1.1	0.14	183
	□ sd	0.3	0.07	82
	* min - max	0.7 - 4.0	0.07 - 0.47	40 - 360
Las flood	□ average	3.3	2.9	85
	□ sd	2.1	4.3	41
	* min - max	0.8 - 6.8	0.1 - 14.9	17 - 174
Rhône river baseflow	average	1.9	0.57	36
Rhône river flood	average	2.8	7.4	16
Huveaune river baseflow	average	1.3	1.0	110
Huveaune river flood	average	4.8	13.8	69
Jarret river baseflow	average	1.8	3.0	230
Jarret river flood	average	6.4	20.9	91
Eygoutier river baseflow	average	4.1	3.1	240
Eygoutier river flood	average	17	39	150

329

330

331 Dissolved and particulate trace metal concentrations

332 The average and variation range of trace metal concentrations during the base flow and flood for the Las River
 333 compared to the rivers from the same part of Mediterranean coast (Rhône, Huveaune, Jarret, and Eygoutier Rivers), and
 334 to the world average and upper continental crust are provided in Table 3 for dissolved TM and in Table SI 5 for
 335 particulate TM content.

336

337 *Dissolved trace metal concentrations (D_{TM})*

338 For most of the D_{TM} in the Las River, the values are in the same range of concentrations during the base flow and the
 339 flood, except for Cr, Co and Zn, for which the two regimes are statistically different ($p < 0.05$, Mann-Whitney) with an
 340 increase by a factor 2. This is also the case for Al with an increase by a factor 3. An hypothesis to explain this increase
 341 could be the presence of colloids of aluminium oxids from clays minerals weathering and their association with Cr, Co
 342 and Zn. Although concentrations of Pb between the base flow and the flood are not statistically different (due to high
 343 variability), it should be highlighted that average Pb concentrations are by factor 2 higher during the flood. Despite
 344 being an urban river, according to D_{TM} , the Las River could be characterised by a non-polluted karstic river. Indeed, all
 345 mean concentrations are below the European Quality Standards (EQS) except for Cu under flood regime (Table 3).
 346 Compared to the world’s river averages, D_{TM} concentrations are higher for Zn, equivalent for Pb and lower for all other
 347 metals.

349 **Table 3.** Dissolved concentration of trace elements (in $\mu\text{g L}^{-1}$) in Las River during base flow and flood, Rhône River
 350 (Ollivier et al. 2011), Huveaune and Jarret Rivers (Oursel et al., 2013; Oursel et al., 2014), Eygoutier River (Nicolau et
 351 al., 2012), European Quality Standards (EQS), world river average (Gaillardet et al., 2003; Viers et al., 2009). For Las
 352 River, “§” refers to average and sd without extremes values, “*” refers to min-max values including extremes values.

	Metal Paramete r	Cd	Pb	Cr	Co	Ni	Cu	Zn	As	Al
Dissolved in $\mu\text{g L}^{-1}$										
Las base flow	§ average	0.018	0.09	0.15	0.03	0.28	0.89	2.83	0.24	4.3
	§ sd	0.007	0.06	0.03	0.01	0.08	0.41	1.98	0.06	2.9
	* min -	0.010 -	0.03 -	0.10 -	0.02 -	0.15 -	0.34 -	0.59 -	0.15 -	0.8 -
	max	0.046	0.24	0.36	0.07	0.48	1.82	6.90	0.33	54.0
Las flood	§ average	0.017	0.21	0.25	0.07	0.26	1.46	6.37	0.23	12.6
	§ sd	0.008	0.20	0.15	0.03	0.07	1.26	4.67	0.06	8.1
	* min -	0.005 -	0.01 -	0.10 -	0.02 -	0.16 -	0.34 -	0.45 -	0.13 -	2.0 -
	max	0.031	0.64	0.61	0.12	0.41	4.53	16.63	0.33	26.1
Rhône base flow	average	-	0.066	-	-	0.763	2.351	3.595	-	-
Rhône flood	average	-	0.070	-	-	1.057	1.970	2.353	-	-
Huveaune base flow	average	0.008	0.13	-	0.41	2.52	1.72	3.40	-	-
Huveaune flood	average	0.021	0.31	-	0.24	1.59	5.02	17.65	0.74	-
Jarret base flow	average	0.008	0.08	-	0.24	1.70	1.78	4.77	-	-
Jarret flood	average	0.025	0.35	-	0.14	1.12	5.59	18.30	0.68	-
Eygoutier base flow	average	0.040	0.60	-	-	-	3.49	18.30	-	-
Eygoutier flood	average	0.006	1.16	-	-	-	3.30	1.31	-	-
EQS	average	0.25	1.2	3.4	-	4	1	7.8	0.83	-
world average base flow	average	0.080	0.08	0.7	0.15	0.80	1.48	0.60	0.62	32

353

354 *Particulate trace metal content in SPM (P_{TM})*

355 Particulate trace metal content (P_{TM}) observed in the Las River (Table SI 5) presents a small range of variation (0.4-fold
 356 for Cd and Cu to 1.8-fold for Co and 2.5-fold for Al) between the base flow and the flood. Nevertheless, for Cd, Cr, Co,
 357 Ni, Cu, As and Al the two periods are statistically different ($p < 0.05$, Mann-Whitney). For Cd and Cu, this difference
 358 consists of a decrease by a factor 2.5 of content during the flood, whereas it corresponds to a relative increase for Cr,
 359 Co, Ni, As and Al. Thus, the particles brought to the sea by the river during a flood are richer in Cr, Co, Ni, Zn and As,
 360 increasing the net mass contribution. This contribution could be associated with the average urban particle signature
 361 taking into account these five elements (Kaonga et al. 2021).

362 For any of the considered metals, no regularity could be extracted for the base flow and the flood events, between
 363 different rivers and the world averages. A short description of P_{TM} tendencies is provided in Table SI 6.

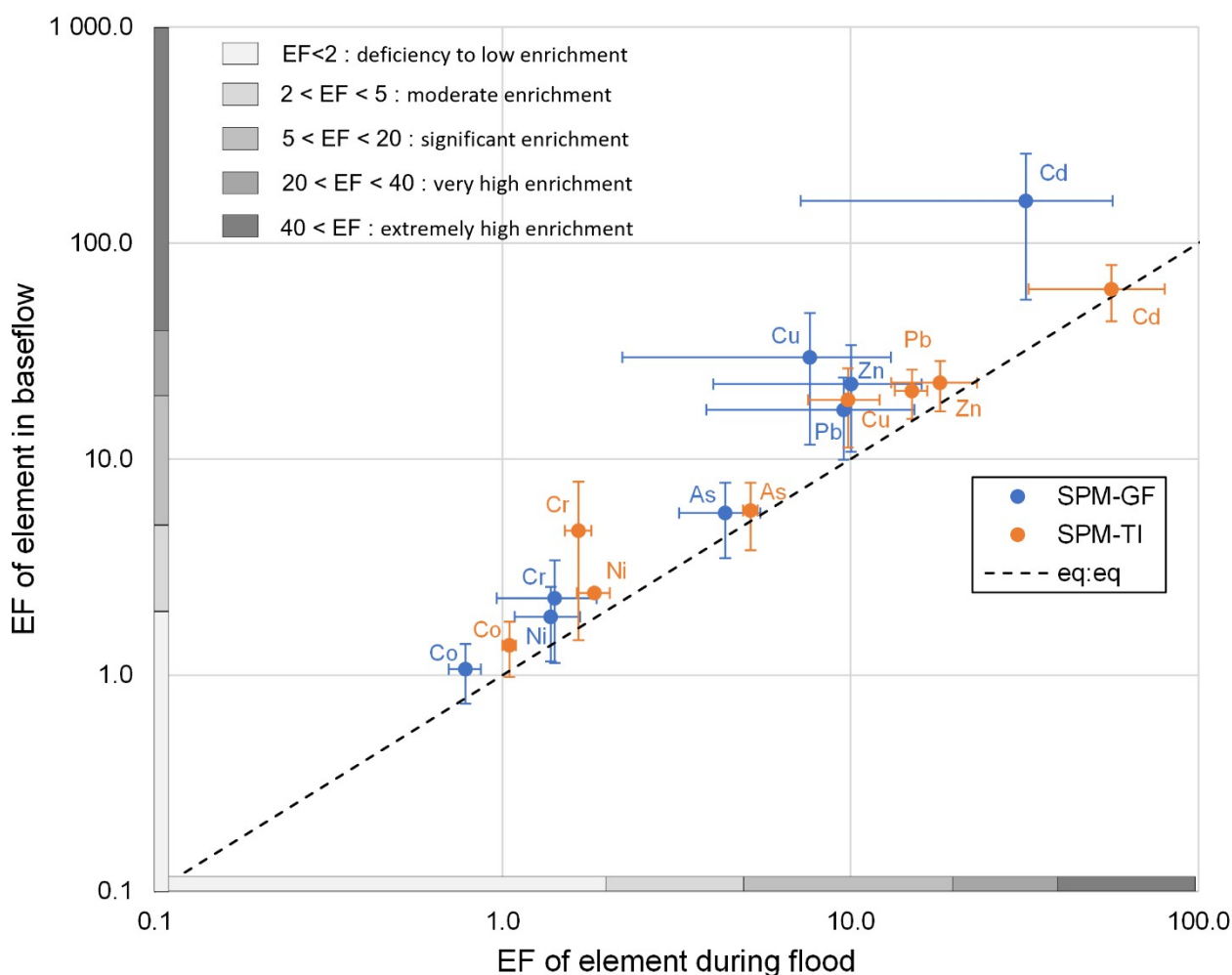
364 Lastly, it stands that all metal contents in SPM are above the UCC average whatever the period except Co. Moreover
 365 Cd, Cu, Zn and Pb are over or in the range of the world's river average content. So an enrichment factor of these
 366 elements in Las River SPM calculation will give more information concerning possible anthropogenic inputs.

367

368 *Enrichment Factor (EF)*

369 Average enrichment factors for measured elements for the base flow, the flood event and for SPM collected by discrete
 370 (SPM_{GF}) and time integrative (SPM_{TI}) sampling are presented in Fig. 2. Among the eight studied elements Co showed
 371 the lowest EF ($EF < 2$) indicating the absence of the anthropogenic contribution, while the highest EF was obtained for
 372 Cd ($EF > 150$; for SPM_{GF}). Therefore, high EF of Cd indicates a potential strong anthropogenic influence or a different
 373 composition of the weathered rocks/soils compared to UCC composition. Assuming that the carbonate background of

374 the watershed is composed mainly of limestone and dolomite (Durozoy et al., 1974; El Houssainy, 2020), there is high
 375 probability that dolomites are enriched in Cd, as it was already found for other karstic carbonate regions (Cuculić et al.,
 376 2009; Vukosav et al., 2014). Enrichment factors for all metals are higher in samples collected during the base flow. This
 377 trend has already been observed in other rivers (Benoit et al., 1994; Miller et al., 2003). This indicates that during flood
 378 the particles are less enriched than during the base flow. This could be linked to the weathering of more crustal material
 379 containing less metals (Cobelo-García & Prego, 2004; Ollivier et al., 2011). This is supported by an increase of Al
 380 content during flood (Table SI 6) and the statistical test of difference (Mann-Whitney test) conducted between the
 381 average EF of SPM_{GF} , indeed for all TM a statistical difference is observed between flood and base flow regime ($p <$
 382 0.05) except for As.



383
 384 **Figure 2.** Average Enrichment Factors (EF) of measured elements relative to Al content and UCC composition
 385 (Rudnick & Gao, 2014). EF is plotted in log scale during baseflow as a function of EF in log scale during flood for
 386 punctual SPM_{GF} particles (blue) and integrated SPM_{TI} (orange). Dotted line represents equivalent distribution. Colour
 387 scale of the EF legend is described on the left and corresponds to the colour of the axes. Error bars represent one
 388 standard deviation.

389
 390 EF observed for the Las River are higher than those observed in the Rhône River (Ollivier et al., 2011) due to an higher
 391 urban surface in Las River watershed (about 30% for Las River against 3.8% for Rhône River). In the Rhône River only
 392 Pb, Cd and Zn were considered as enriched (EF higher than 3) whereas Cu, Ni, Co and Cr were around 1.5. Using
 393 average data from Table SI 6, enrichment factors were calculated for trace metals in Las, Huveaune, Jarret, Eygoutier
 394 and Rhône Rivers during base flow and flood and compared to the average world river SPM (Table SI 7). For Cd, Pb,

395 Cu, Zn and As in Huveaune River and Cd, Cu and Zn in Jarret River we observed a very high enrichment factor and an
396 extremely high enrichment of Pb in the Jarret River which is the most urbanised watershed (about 50%). In general,
397 during floods EF is less important in the Las River than in the Huveaune and Jarret, but higher than in Rhône River
398 which is the less urbanised catchment.

399 Fig. 2 also points out the differences between SPM_{GF} and SPM_{TI} . For all metals, the EFs during the flood were higher for
400 particles collected using time-integrated passive sampler (SPM_{TI}) than for grab samples (SPM_{GF}). Nevertheless, this
401 difference is only significant for Co, Ni and Zn (Mann-Whitney, $p < 0.05$). This difference was attributed to the
402 difference of sampling method and possible variability in the SPM composition (Lučić et al., 2019, 2021). This could
403 also be related to the particles size, as in average the lower grain size with the higher specific surface is collected using
404 integrative sampler. During base flow, mean EF are similar whatever the way particles were collected, for all metals
405 except Cd, Cr and Co.

406

407 Partitioning between particulate and dissolved fraction

408 The partitioning of trace metals based on the calculation of the distribution coefficient (K_D) was studied to estimate
409 whether the composition of particles is changing upon the different flow regimes. The percentages of particulate
410 fractions as a function of SPM_{GF} , along with the theoretical lines representing the different distribution coefficients are
411 plotted in Fig. 3 and Fig. SI 8.

412 From a general point of view, elements can be grouped depending on their different $\log K_D$. Arsenic presents a $\log K_D$
413 around 4.6 (Fig. 3-A), Zn, Cu, Ni, Co, and Cd have a $\log K_D$ around 5 (Fig. 3-B, example of Cu), Cr around 5.5 (Fig. 3-
414 C) and Pb around 6 (Fig. 3-D).

415 The optimised $\log K_D$ are similar for the flood and the base flow for Cr, Co and Zn but different for Cd, Cu, As, Ni and
416 Pb. This indicates different interaction properties of particles with respect to these trace metals. Cd and Cu have a
417 higher K_D during the base flow than during the flood, whereas it is the opposite for Pb, As and Ni (Fig. 3 and Fig. SI 7).
418 Cobelo-García et al. (2004) described a negative relation between K_D of trace metals and SPM concentrations explained
419 by an organic rich SPM predominant during base flow and a detrital SPM, poor in metals and increasing with flow.
420 (Ollivier et al. 2011) also presented this relation with a negative trend for some metals (Ni and Cu) and not significant
421 for Zn and Pb. This negative trend could also be related to the effect of the particle concentration on the trace metal
422 partition between the water and particles, named "particle concentration effect" as discussed by (Benoit & Rozan
423 1999), with a various of causes. In our case, a negative trend is observed for Cd, Cu and Zn.

424 The optimised $\log K_D$ for Cu, Pb, Cd and Zn are consistent with literature (Cobelo-García et al., 2004; Deycard et al.,
425 2014; Miller et al., 2003; Ollivier et al., 2011; Oursel et al., 2014). Copper is known to have a great affinity for organic
426 matter. POC content being higher during base flow in the Las River but also in other rivers (Table 2), this could explain
427 the higher $\log K_D$ of Cu during base flow compared to flood (Fig. 3-B).

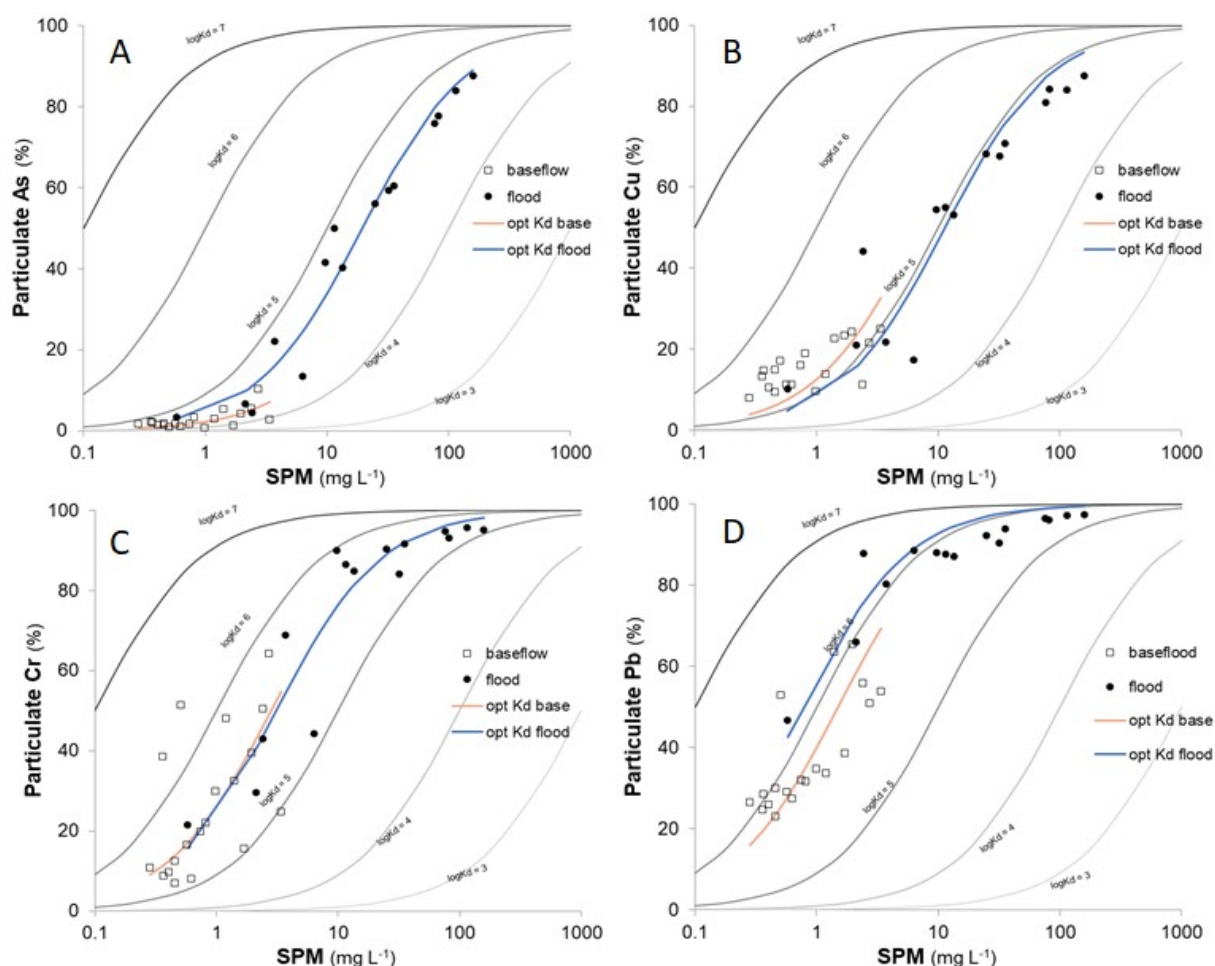
428 The optimised $\log K_D$ for Co are consistent with the values from (Miller et al., 2003) under base flow (5.0) but slightly
429 higher than those observed during the flood compared to the Huveaune and Jarret rivers (Oursel et al., 2014).

430 Concerning Ni and Cr, the $\log K_D$ are significantly higher than the one observed in previous works and seem not to be
431 influenced by the hydrologic regime (Miller et al., 2003; Oursel et al., 2014).

432 Finally, $\log K_D$ for As is the lowest in this study and it is consistent with value of Oursel et al. (2014) in Huveaune and
 433 Jarret rivers (3.9) and of Miller et al. (2003) in Chesterville Branch (4.4).

434 From Fig. 3 it can be noted that the percentage of particulate metal increases with increasing SPM concentration
 435 following the optimised $\log K_D$ of each metal. So, according to the optimised $\log K_D$ calculated under flood, particulate
 436 metals become prevailing over the dissolved ones at SPM concentration of above 20, 15, 3, 1 mg L⁻¹, for As, Cu, Cr and
 437 Pb, respectively. It is therefore clear that during the flood Cr and Pb load is dominated by the particulate fraction.

438



439

440 **Figure 3.** Selected Particulate TM concentration in % as a function of SPM_{GF} concentration (mg L⁻¹) in log
 441 scale. Empty square represents base flow data and black disc represents flood. Black lines represent
 442 theoretical lines for $\log K_D$, blue line represents optimised $\log K_D$ during flood and orange line represents
 443 optimised $\log K_D$ during base flow. The Quadrant B for Cu is representative of Zn, Ni, Co, and Cd patterns.

444

445 Trace metal fluxes

446 Fluxes of trace metals are calculated for two hydrological annual periods: March 2017 to March 2018 (period 1) and
 447 March 2018 to March 2019 (period 2), presenting different meteorological conditions (Table 4). The rainfall for the
 448 second period (785 mm) was twice the former one (356 mm). As a results, the volume of water and the SPM load
 449 delivered by the Las River due to floods are different during the two periods. Between periods 1 and 2, the water and
 450 SPM load are 6 and 4 times higher, respectively (Table 4). On the contrary under baseflow conditions, the volume of
 451 water is quite similar during the two annual periods, while the SPM load is 3 times higher during the period 2 compared

452 to the period 1 (Table 4). The values of SPM and flow are consistent with those found by Dufresne et al. (2020) for a
453 year in 2013 (SPM: 707 t y⁻¹ and flow: 58 Mm³ y⁻¹).

454

455 **Table 4.** Hydrological conditions during the two studied periods.

	3/2017-3/2018 (period 1)		3/2018-3/2019 (period 2)	
	Base flow	Flood	Base flow	Flood
volume (×10 ⁶ m ³)	8.1	4.9	7.9	30
SPM (×10 ⁶ g)	15	185	54	777
Rain (mm)		356		785

456

457 The annual load of each studied TM for the two separate periods are represented in Fig. 4, distinguishing base flow and
458 flood on separate histograms and indicating on each histogram the proportion of particulate and dissolved load. For
459 period 1 (3/17 to 3/18), the flood inputs are dominant and represents from 50 % to 87 %, for As to Pb, respectively. It
460 seems consistent because As is predominantly delivered in a dissolved form irrespective of the hydrologic regime and
461 Pb is predominantly delivered under particulate form for any hydrologic regime. During period 2 (3/18 to 3/19), the
462 flood inputs are also dominant representing from 87 % to 92 %, from As to Pb, respectively.

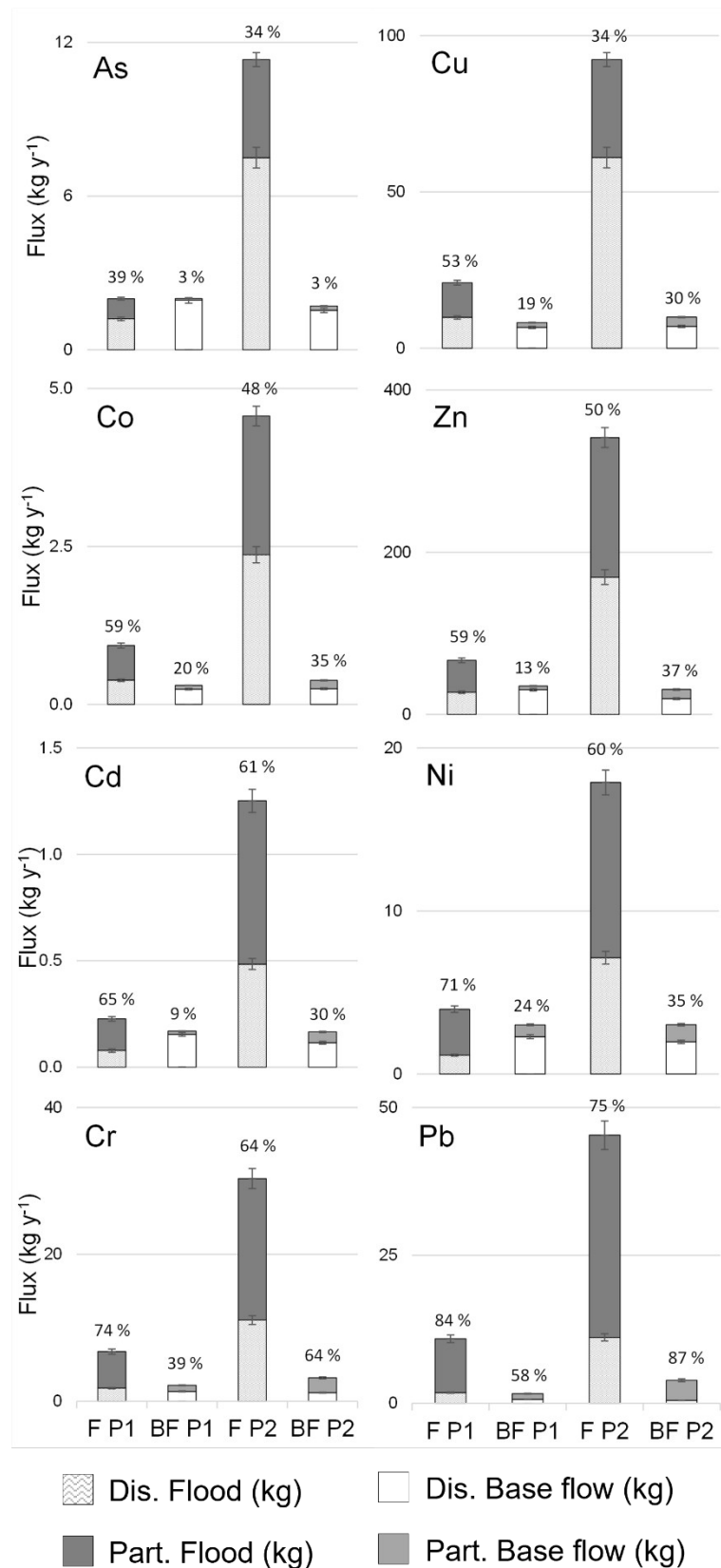
463 Taking into account the mean of the 2 years of the study, during the base flow period, Cd, Co, Ni, Cu, Zn and As are
464 predominantly loaded under dissolved form (from 70 % for Ni to 93 % for As). Only Pb and Cr are predominantly
465 delivered in particulate form with only 21 and 46 % under dissolved form respectively. These results are in accordance
466 with the K_D and the lower concentration of SPM under base flow regime. During flood, Cd, Pb, Cr and Ni prevailed
467 under particulate form (respectively 62, 77, 65 and 62 %), Co and Zn are equally distributed (respectively 50 and 52 %)
468 and lastly Cu and As prevailed in dissolved form (respectively 38 and 35 %). For Pb, Cr and As these findings are
469 consistent with the optimised $\log K_D$ determined. For metals like Cu ($\log K_D$ around 5) the correlation between K_D and
470 percentage in particulate form is probably subjected to large uncertainty hiding the theoretical trend.

471

472

473

474

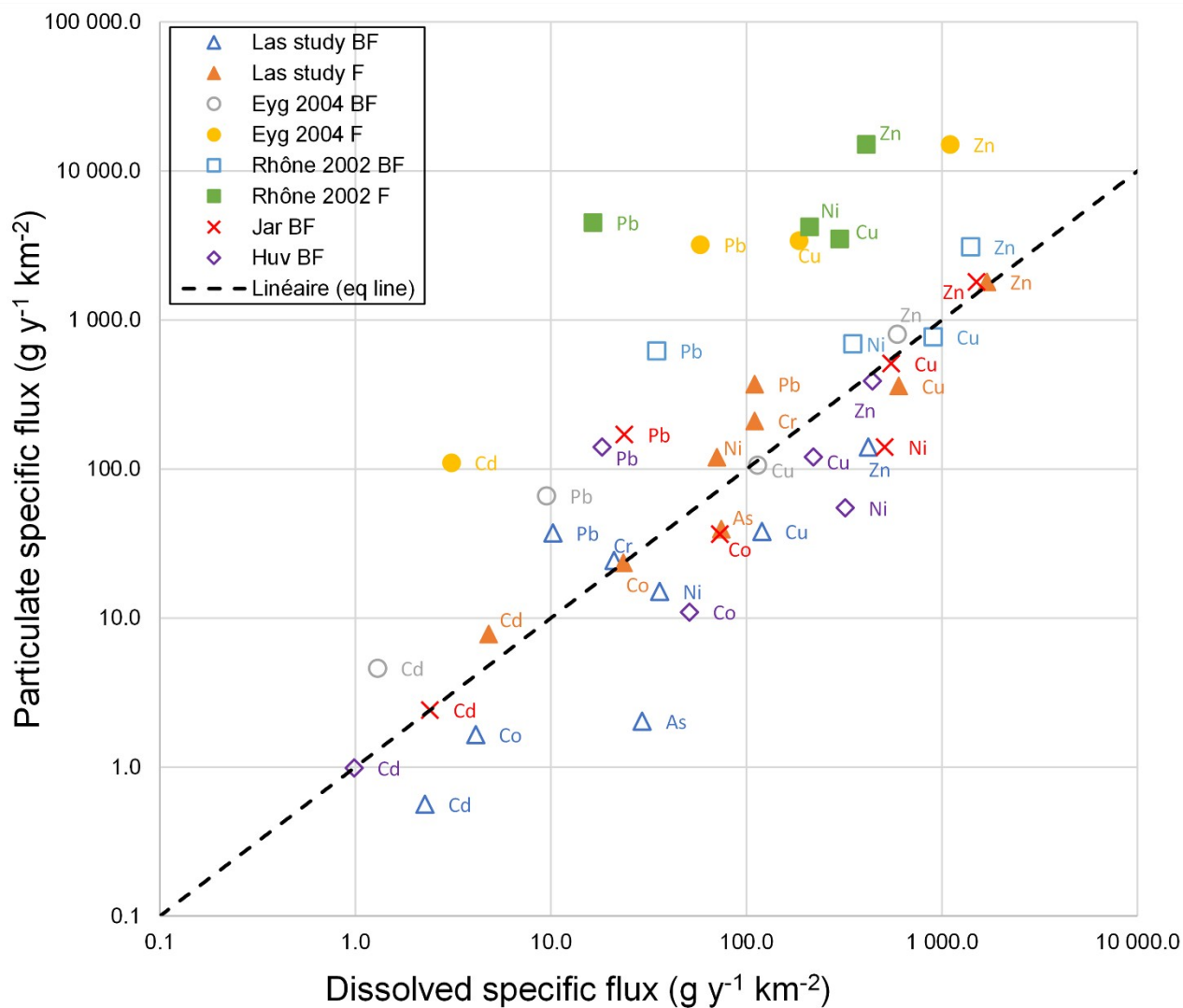


475

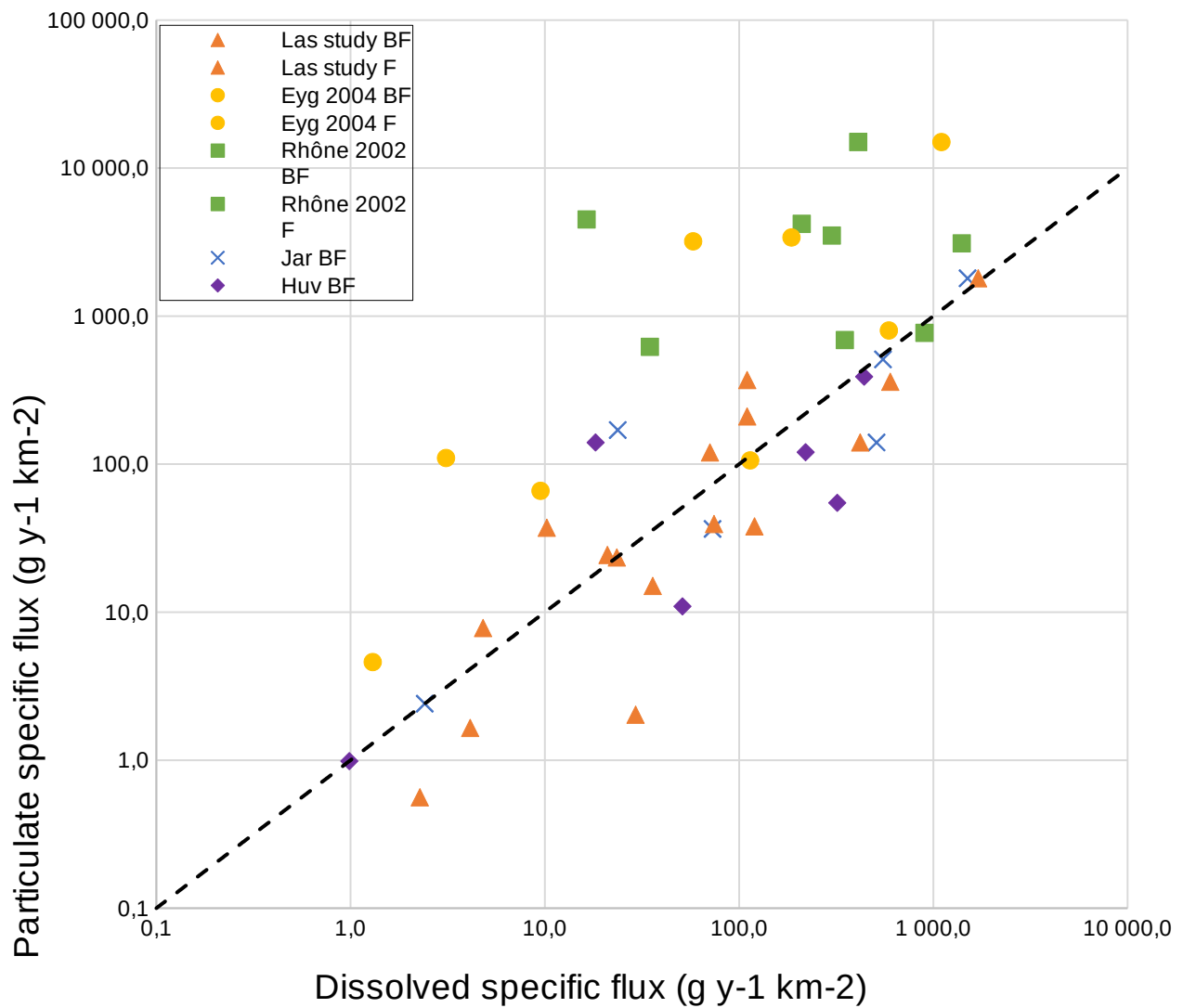
476 **Figure 4.** Annual TM load in kg y^{-1} during two periods March 2017 to March 2018 (P1) and March 2018 to March
 477 2019 (P2) for selected TM (As, Cu, Cr and Pb). For each period load is separated into flood and baseflow. On flood (F)
 478 histogram dark grey represents particulate load and wavy plot represents dissolved load. On the base flow (BF)
 479 histogram grey represents particulate load and white represents dissolved load. Errors bars represent 5 % of the value
 480 for dissolved fraction and 7 % of the value for particulate fraction. Value (in %) above each histogram refers to the
 481 particulate % in the histogram.

482

483



484



485

486 **Figure 5.** Dissolved and particulate specific flux (in g y⁻¹ km⁻²) for Cd, Pb, Co, Ni, Cu, Zn, As, Cr in Las River (this
 487 study) and other small and large Mediterranean rivers during base flow and flood (Nicolau et al., 2012; Ollivier et al.,
 488 2011; Oursel et al., 2013). Empty forms represent base flow data (BF) and full forms represent flood (F).

489

490 The specific fluxes, meaning annual load divided by the watershed surface (Nicolau et al., 2012; Ollivier et al., 2011),
 491 allowed us to compare rivers of different watersheds. Contrasting patterns were obtained for dissolved metals under
 492 base flow (Fig.5). Specific cadmium flux in the Las River is equivalent to Jarret River (both are urban rivers), but it is
 493 significantly higher than the flux of the Eygoutier River (less urban river and less calcareous area than Las River). For
 494 Pb all specific fluxes are in the same range, highlighting no difference in terms of sources of contamination between
 495 these catchments. For Co, Ni and As, the Las River is less contaminated than other surrounding watersheds. In the Las
 496 River, Cu and Zn fluxes are relatively equal to those found in the Eygoutier and Huveaune Rivers, but clearly lower
 497 than in the Jarret and Rhone Rivers. During flood comparison with the Rhone River changes. Contamination by Pb, Cu
 498 and Zn became predominant in the Las River whereas for Ni and As, the Rhône River is predominant (Fig. 5).

499 For all particulate metals under the base flow specific fluxes are in the same range of values as for the Eygoutier and
 500 Huveaune Rivers, but significantly lower than in the Jarret and Rhône Rivers (Fig. 5). A comparison with the Rhône
 501 River during the flood indicates a greater load of trace metals per km² related to the 10 times higher specific SPM flux

502 of the Rhône River (Table SI 7). So, an extrapolation of our results to other Mediterranean rivers should be conducted
503 with care as, the SPM can play an important role.

504 Contribution to the bay

505 From these particulate and dissolved fluxes, an estimation of contribution of the Las River trace metal inputs is
506 calculated. These values are compared to the stock of trace metals in the upper (0-5 cm) sediment estimated in the little
507 Bay of Toulon Bay (Tessier et al., 2011) for the particulate fraction. For the dissolved fraction these values are
508 compared to an estimation stock of dissolved trace metals in the little bay, from concentrations measured in 2017 in
509 surface (unpublished data) as described by Coclet et al., 2018 and extrapolated to the whole volume. As a result, the
510 annual particulate contribution of the Las River is less than 0.2 % for Cu, Pb, Zn (Table SI 9), so Las River is not the
511 main contributor to the sediment contamination in the little bay. The annual dissolved contribution of the Las River
512 varies among trace metals. For Cd, Pb, Cr, Ni, Cu and Zn it is between 21 and 48 %, around 4 % for As and 115 % for
513 Co (Table SI 9). In these conditions the contribution of the Las River appears as not negligible, compared to the water
514 column stock.

515 Conclusions

516 This work highlights the importance of sampling strategy for small river studies. First, high-frequency monitoring of
517 flow and turbidity as a proxy of suspended particulate matter is necessary to correctly account for these two key
518 parameters. For chemical measurements monthly sampling during base flow was sufficient to obtain a correct annual
519 load. However, it was important to consider flood differently than base flow (focus on flood). For floods, a relation
520 between flux and flow can be used that allows extrapolation to unsampled flood events. The use of time-integrated SPM
521 sampler allowed periodic collection of representative particles.

522 The results point out that for small Mediterranean rivers the flood represents the main regime for trace metal load (from
523 78 % for As to 91 % for Pb) even if it occurs only 20 % of the time. Moreover, the impact of the flood was mainly
524 dependent on the SPM flux and on the flow intensity. Indeed, a 2-fold increase in precipitation leads to an increase in
525 volume and SPM discharge by a factor of 4 to 6 and consequently to a corresponding increase in TM load depending on
526 its main affinity for dissolved fractions (e.g. As increase for the same volume increase) or particulate fractions (e.g Pb
527 increase for the same SPM increase). It was also found that the yield of As, Cu, Co, Zn, Cd and Ni during base flow was
528 mainly in the dissolved phase and for Pb in the particulate phase. During flood, the yield of As was mainly in the
529 dissolved phase, while the yield of Cd, Ni, Cr and Pb was in the particulate phase. A decrease in the enrichment factor
530 for all trace metals was observed from base flow to flood probably due to more neutral particles coming from the
531 watershed erosion. Compared to other watersheds, we conclude that the specific dissolved fluxes for some metals could
532 be higher in small rivers, but for the specific particulate fluxes the importance of SPM concentrations should be
533 considered. Extrapolation of results from one catchment to a larger zone should therefore be considered with caution. In
534 terms of contribution to the small bay, particulate trace metals annual yield is low compared to the high contamination
535 of the sediment while dissolved trace metals annual input represents, for Cd, Pb, Cr, Ni, Cu and Zn 20 to 50 % of the
536 dissolved stock.

537

538 References

539 Audement, C., Arfib, B., Mazzilli, N., Jouvès, J., Lamarque, T., & Guglielmi, Y. (2017). Groundwater management
540 of a highly dynamic karst by assessing baseflow and quickflow with a rainfall-discharge model (Dardennes

- 541 springs, SE France). *Bulletin de la Société géologique de France*, 188(6), 40.
 542 <https://doi.org/10.1051/bsgf/2017203>
- 543 Benoit, G., Oktay-Marshall, S. D., Cantu, A., Hood, E. M., Coleman, C. H., Corapcioglu, M. O., & Santschi, P. H.
 544 (1994). Partitioning of Cu, Pb, Ag, Zn, Fe, Al, and Mn between filter-retained particles, colloids, and solution
 545 in six Texas estuaries. *Marine Chemistry*, 45(4), 307–336. [https://doi.org/10.1016/0304-4203\(94\)90076-0](https://doi.org/10.1016/0304-4203(94)90076-0)
- 546 Benoit, Gaboury, & Rozan, T. F. (1999). The influence of size distribution on the particle concentration effect and
 547 trace metal partitioning in rivers. *Geochimica et Cosmochimica Acta*, 63(1), 113–127.
 548 [https://doi.org/10.1016/S0016-7037\(98\)00276-2](https://doi.org/10.1016/S0016-7037(98)00276-2)
- 549 Bernal, S., von Schiller, D., Sabater, F., & Martí, E. (2013, November). Hydrological extremes modulate nutrient
 550 dynamics in mediterranean climate streams across different spatial scales. *Hydrobiologia*.
 551 <https://doi.org/10.1007/s10750-012-1246-2>
- 552 Bello-García, A., & Prego, R. (2004). Influence of point sources on trace metal contamination and distribution in
 553 a semi-enclosed industrial embayment: the Ferrol Ria (NW Spain). *Estuarine, Coastal and Shelf Science*,
 554 60(4), 695–703. <https://doi.org/10.1016/J.ECSS.2004.03.008>
- 555 Bello-García, A., Prego, R., & Labandeira, A. (2004). Land inputs of trace metals, major elements, particulate
 556 organic carbon and suspended solids to an industrial coastal bay of the NE Atlantic. *Water Research*, 38(7),
 557 1753–1764. <https://doi.org/10.1016/j.watres.2003.12.038>
- 558 Bclet, C., Garnier, C., Delpy, F., Jamet, D., Durrieu, G., Le Poupon, C., et al. (2018). Trace metal contamination as
 559 a toxic and structuring factor impacting ultraphytoplankton communities in a multicontaminated
 560 Mediterranean coastal area. *Progress in Oceanography*, 163, 196–213.
 561 <https://doi.org/10.1016/j.pocean.2017.06.006>
- 562 Bclet, C., Garnier, C., Durrieu, G., D'Onofrio, S., Layglon, N., Briand, J. F., & Misson, B. (2020). Impacts of copper
 563 and lead exposure on prokaryotic communities from contaminated contrasted coastal seawaters: The
 564 influence of previous metal exposure. *FEMS Microbiology Ecology*, 96(6).
 565 <https://doi.org/10.1093/femsec/fiaa048>
- 566 Bclet, C., Garnier, C., Durrieu, G., Omanović, D., D'Onofrio, S., Le Poupon, C., et al. (2019). Changes in
 567 Bacterioplankton Communities Resulting From Direct and Indirect Interactions With Trace Metal Gradients
 568 in an Urbanized Marine Coastal Area. *Frontiers in Microbiology*, 10(FEB), 257.
 569 <https://doi.org/10.3389/fmicb.2019.00257>
- 570 Bowling, R. M., Ojeda, F., Lamont, B. B., Rundel, P. W., & Lechmere-Oertel, R. (2005). Rainfall reliability, a
 571 neglected factor in explaining convergence and divergence of plant traits in fire-prone mediterranean-
 572 climate ecosystems. *Global Ecology and Biogeography*, 14(6), 509–519. <https://doi.org/10.1111/J.1466-822X.2005.00166.X>
- 573
- 574 Čulić, V., Cukrov, N., Kwokal, Ž., & Mlakar, M. (2009). Natural and anthropogenic sources of Hg, Cd, Pb, Cu and
 575 Zn in seawater and sediment of Mljet National Park, Croatia. *Estuarine, Coastal and Shelf Science*, 81(3),
 576 311–320. <https://doi.org/10.1016/j.ecss.2008.11.006>
- 577
- 578 Dang, D. H., Schäfer, J., Brach-Papa, C., Lenoble, V., Durrieu, G., Dutruch, L., et al. (2015). Evidencing the Impact
 579 of Coastal Contaminated Sediments on Mussels Through Pb Stable Isotopes Composition. *Environmental
 Science and Technology*, 49(19), 11438–11448. <https://doi.org/10.1021/acs.est.5b01893>
- 580
- 581 Meycard, V. N., Schäfer, J., Blanc, G., Coynel, A., Petit, J. C. J., Lancelier, L., et al. (2014). Contributions and
 582 potential impacts of seven priority substances (As, Cd, Cu, Cr, Ni, Pb, and Zn) to a major European Estuary
 583 (Gironde Estuary, France) from urban wastewater. *Marine Chemistry*, 167, 123–134.
 584 <https://doi.org/10.1016/j.marchem.2014.05.005>

- 584 Lufresne, C. (2014). *Compréhension et analyse des processus hydro-sédimentaires de la Baie de Toulon. : Apport*
585 *à la modélisation de la dispersion des radionucléides*. Ph. D. Université de toulon.
- 586 Lufresne, C., Arfib, B., Ducros, L., Duffa, C., Giner, F., & Rey, V. (2020). Karst and urban flood-induced solid
587 discharges in Mediterranean coastal rivers: The case study of Las River (SE France). *Journal of Hydrology*,
588 590. <https://doi.org/10.1016/j.jhydrol.2020.125194>
- 589umas, C., Ludwig, W., Aubert, D., Eyrolle, F., Raimbault, P., Gueneugues, A., & Sotin, C. (2015). Riverine transfer
590 of anthropogenic and natural trace metals to the Gulf of Lions (NW Mediterranean Sea). *Applied*
591 *Geochemistry*, 58, 14–25. <https://doi.org/10.1016/J.APGEOCHEM.2015.02.017>
- 592urozoy, G., Gouvernet, C., & Jonquet, P. (1974). *Ministère de l'industrie, Bureau de Recherches Géologiques et*
593 *Minières, Service géologique national, Notice explicative Echelle: 1/50000 Service géologique régional*
594 *Provence-Corse*.
- 595Houssainy, A. (2020). *Apports et géochimie sédimentaire des éléments traces métalliques dans deux zones*
596 *côtières méditerranéennes urbanisées : Beyrouth (Liban) et Toulon (France)*. Université de Toulon.
- 597ang, T. H., & Chen, W. H. (2021). Dissolved and particulate nitrogen species partitioning and distribution in the
598 Danshuei River estuary, northern Taiwan. *Marine Pollution Bulletin*, 164.
599 <https://doi.org/10.1016/j.marpolbul.2021.111981>
- 600aillardet, J., Viers, J., & Dupré, B. (2003). Trace Elements in River Waters. In *Treatise on Geochemistry* (Vol. 5–9,
601 pp. 225–272). Elsevier. <https://doi.org/10.1016/B0-08-043751-6/05165-3>
- 602alloway, J. N., Aber, J. D., Erisman, J. W., Seitzinger, S. P., Howarth, R. W., Cowling, E. B., & Cosby, B. J. (2003).
603 The Nitrogen Cascade. *BioScience*, 53(4), 341–356.
- 604onzález-Ortegón, E., Laiz, I., Sánchez-Quiles, D., Cobelo-García, A., & Tovar-Sánchez, A. (2019). Trace metal
605 characterization and fluxes from the Guadiana, Tinto-Odiel and Guadalquivir estuaries to the Gulf of Cadiz.
606 *Science of the Total Environment*, 650, 2454–2466. <https://doi.org/10.1016/j.scitotenv.2018.09.290>
- 607amarque, T. (2014). *Établissement d'une courbe de tarage des débits du cours d'eau du Las réalisée d'août à*
608 *décembre 2013*.
- 609ayglon, N., Misson, B., Durrieu, G., Coclet, C., D'Onofrio, S., Dang, D. H., et al. (2020). Long-term monitoring
610 emphasizes impacts of the dredging on dissolved Cu and Pb contamination along with ultraplankton
611 distribution and structure in Toulon Bay (NW Mediterranean Sea, France). *Marine Pollution Bulletin*, 156.
612 <https://doi.org/10.1016/j.marpolbul.2020.111196>
- 613rrain, A., Savoye, N., Chauvaud, L., Paulet, Y. M., & Naudet, N. (2003). Decarbonation and preservation method
614 for the analysis of organic C and N contents and stable isotope ratios of low-carbonated suspended
615 particulate material. *Analytica Chimica Acta*, 491(2), 125–133. [https://doi.org/10.1016/S0003-](https://doi.org/10.1016/S0003-2670(03)00815-8)
616 [2670\(03\)00815-8](https://doi.org/10.1016/S0003-2670(03)00815-8)
- 617ičić, M., Jurina, I., Ščančar, J., Mikac, N., & Vdović, N. (2019). Sedimentological and geochemical
618 characterization of river suspended particulate matter (SPM) sampled by time-integrated mass flux sampler
619 (TIMS) in the Sava River (Croatia). *Journal of Soils and Sediments*, 19(2), 989–1004.
620 <https://doi.org/10.1007/s11368-018-2104-2>
- 621ičić, M., Mikac, N., Bačić, N., & Vdović, N. (2021). Appraisal of geochemical composition and hydrodynamic
622 sorting of the river suspended material: Application of time-integrated suspended sediment sampler in a
623 medium-sized river (the Sava River catchment). *Journal of Hydrology*, 597, 125768.
624 <https://doi.org/10.1016/J.JHYDROL.2020.125768>

- 625 Keybeck, M. (2001). River sediment transport and quality: From space and time variability to management.
626 *Houille Blanche*, (6-7), 34-43. <https://doi.org/10.1051/lhb/2001067>
- 627 Miller, P. C. (1983). Canopy Structure of Mediterranean-Type Shrubs in Relation to Heat and Moisture, 133-166.
628 https://doi.org/10.1007/978-3-642-68935-2_8
- 629 Miller, C. V., Foster, G. D., & Majedi, B. F. (2003). Baseflow and stormflow metal fluxes from two small
630 agricultural catchments in the Coastal Plain of the Chesapeake Bay Basin, United States. *Applied*
631 *Geochemistry*, 18(4), 483-501. [https://doi.org/10.1016/S0883-2927\(02\)00103-8](https://doi.org/10.1016/S0883-2927(02)00103-8)
- 632 Misson, B., Garnier, C., Lauga, B., Dang, D. H., Ghiglione, J. F., Mullot, J. U., et al. (2016). Chemical multi-
633 contamination drives benthic prokaryotic diversity in the anthropized Toulon Bay. *Science of the Total*
634 *Environment*, 556, 319-329. <https://doi.org/10.1016/j.scitotenv.2016.02.038>
- 635 Colau, R., Lucas, Y., Merdy, P., & Raynaud, M. (2012). Base flow and stormwater net fluxes of carbon and trace
636 metals to the Mediterranean sea by an urbanized small river. *Water Research*, 46(20), 6625-6637.
637 <https://doi.org/10.1016/j.watres.2012.01.031>
- 638 Colau, Rudy. (2005). *Caractérisation et quantification des transferts dus aux petites rivières côtières*
639 *méditerranéennes*. Université de Toulon.
- 640 Grinc, N., Markovics, R., Kanduč, T., Walter, L. M., & Hamilton, S. K. (2008). Sources and transport of carbon and
641 nitrogen in the River Sava watershed, a major tributary of the River Danube. *Applied Geochemistry*, 23(12),
642 3685-3698. <https://doi.org/10.1016/J.APGEOCHEM.2008.09.003>
- 643 ías, M., Cánovas, C. R., Nieto, J. M., & Sarmiento, A. M. (2006). Evaluation of the dissolved contaminant load
644 transported by the Tinto and Odiel rivers (South West Spain). *Applied Geochemistry*, 21(10), 1733-1749.
645 <https://doi.org/10.1016/J.APGEOCHEM.2006.05.009>
- 646 Olivier, P., Radakovitch, O., & Hamelin, B. (2011). Major and trace element partition and fluxes in the Rhône
647 River. *Chemical Geology*, 285(1-4), 15-31. <https://doi.org/10.1016/j.chemgeo.2011.02.011>
- 648 Ursel, B., Garnier, C., Durrieu, G., Mounier, S., Omanović, D., & Lucas, Y. (2013). Dynamics and fates of trace
649 metals chronically input in a Mediterranean coastal zone impacted by a large urban area. *Marine Pollution*
650 *Bulletin*, 69(1-2), 137-149. <https://doi.org/10.1016/j.marpolbul.2013.01.023>
- 651 Ursel, B., Garnier, C., Pairaud, I., Omanović, D., Durrieu, G., Syakti, A. D., et al. (2014). Behaviour and fate of
652 urban particles in coastal waters: Settling rate, size distribution and metals contamination characterization.
653 *Estuarine, Coastal and Shelf Science*, 138, 14-26. <https://doi.org/10.1016/j.ecss.2013.12.002>
- 654 Ursel, B., Garnier, C., Zebracki, M., Durrieu, G., Pairaud, I., Omanović, D., et al. (2014). Flood inputs in a
655 mediterranean coastal zone impacted by a large urban area: Dynamic and fate of trace metals. *Marine*
656 *Chemistry*, 167, 44-56. <https://doi.org/10.1016/j.marchem.2014.08.005>
- 657 telet, E., Luck, J. M., Ben Othman, D., Negrel, P., & Aquilina, L. (1998). Geochemistry and water dynamics of a
658 medium-sized watershed: the Hérault, southern France: 1. Organisation of the different water reservoirs as
659 constrained by Sr isotopes, major, and trace elements. *Chemical Geology*, 150(1-2), 63-83.
660 [https://doi.org/10.1016/S0009-2541\(98\)00053-9](https://doi.org/10.1016/S0009-2541(98)00053-9)
- 661 Hillips, J. M., Russell, M. A., & Walling, D. E. (2000). Time-integrated sampling of fluvial suspended sediment: a
662 simple methodology for small catchments. *Hydrological processes*, 14, 2589-2602.
- 663 ont, D., Simonnet, J. P., & Walter, A. V. (2002). Medium-term Changes in Suspended Sediment Delivery to the
664 Ocean: Consequences of Catchment Heterogeneity and River Management (Rhône River, France).
665 *Estuarine, Coastal and Shelf Science*, 54(1), 1-18. <https://doi.org/10.1006/ECSS.2001.0829>

666 tot, C., Féraud, G., Schärer, U., Barats, A., Durrieu, G., Le Poupon, C., et al. (2012). Groundwater and river
667 baseline quality using major, trace elements, organic carbon and Sr-Pb-O isotopes in a Mediterranean
668 catchment: The case of the Lower Var Valley (south-eastern France). *Journal of Hydrology*, 472–473, 126–
669 147. <https://doi.org/10.1016/j.jhydrol.2012.09.023>

670 oussiez, V., Ludwig, W., Radakovitch, O., Probst, J. L., Monaco, A., Charrière, B., & Buscail, R. (2011). Fate of
671 metals in coastal sediments of a Mediterranean flood-dominated system: An approach based on total and
672 labile fractions. *Estuarine, Coastal and Shelf Science*, 92(3), 486–495.
673 <https://doi.org/10.1016/j.ecss.2011.02.009>

674 dnick, R. L., & Gao, S. (2014). Composition of the Continental Crust. In *Treatise on Geochemistry: Second*
675 *Edition* (Vol. 4, pp. 1–51). Elsevier Inc. <https://doi.org/10.1016/B978-0-08-095975-7.00301-6>

676 mpere, R., Charrière, B., Van Wambeke, F., & Cauwet, G. (2000). Carbon inputs of the Rhône River to the
677 Mediterranean Sea: Biogeochemical implications Carbon inputs of the Rhône River to the Mediterranean
678 Sea: Biogeochemical implications. *Global Biogeochemical Cycles*, 14(2), 669–681.
679 <https://doi.org/10.1029/1999GB900069i>

680 otherland, R. A. (2000). Bed sediment-associated trace metals in an urban stream, Oahu, Hawaii. *Environmental*
681 *Geology* 2000 39:6, 39(6), 611–627. <https://doi.org/10.1007/S002540050473>

682 essier, E., Garnier, C., Mullot, J. U., Lenoble, V., Arnaud, M., Raynaud, M., & Mounier, S. (2011). Study of the
683 spatial and historical distribution of sediment inorganic contamination in the Toulon bay (France). *Marine*
684 *Pollution Bulletin*, 62(10), 2075–2086. <https://doi.org/10.1016/J.MARPOLBUL.2011.07.022>

685 ers, J., Dupré, B., & Gaillardet, J. (2009). Chemical composition of suspended sediments in World Rivers: New
686 insights from a new database. *Science of the Total Environment*, 407(2), 853–868.
687 <https://doi.org/10.1016/j.scitotenv.2008.09.053>

688 kosav, P., Mlakar, M., Cukrov, N., Kwokal, Ž., Pižeta, I., Pavlus, N., et al. (2014). Heavy metal contents in water,
689 sediment and fish in a karst aquatic ecosystem of the Plitvice Lakes National Park (Croatia). *Environmental*
690 *Science and Pollution Research*, 21(5), 3826–3839. <https://doi.org/10.1007/s11356-013-2377-3>

691

692

693